Anal. Chem. **2010,** *82,* 250–257

Sensitive Detection of H_2S Using Gold Nanoparticle Decorated Single-Walled Carbon Nanotubes

Syed Mubeen,[†] Ting Zhang,[†] Nicha Chartuprayoon,[†] Youngwoo Rheem,[†] Ashok Mulchandani,[†] Nosang V. Myung,*[,†] and Marc A. Deshusses*[,‡]

Department of Chemical and Environmental Engineering and Center for Nanoscale Science and Engineering, University of California-Riverside, Riverside, California 92521, and Department of Civil and Environmental Engineering, Duke University, Durham, North Carolina 27708

Herein, we demonstrate that highly sensitive conductometric gas nanosensors for H_2S can be synthesized by electrodepositing gold nanoparticles on single-walled carbon nanotube (SWNT) networks. Adjusting the electrodeposition conditions allowed for tuning of the size and number of gold nanoparticles deposited. The best H_2S sensing performance was obtained with discrete gold nanodeposits rather than continuous nanowires. The gas nanosensors could sense H_2S in air at room temperature with a 3 ppb limit of detection. The sensors were reversible, and increasing the bias voltage reduced the sensor recovery time, probably by local Joule heating. The sensing mechanism is believed to be based on the modulation of the conduction path across the nanotubes emanating from the modulation of electron exchange between the gold and carbon nanotube defect sites when exposed to H_2S.

Sensitive detection and monitoring of gaseous reduced sulfur compounds such as hydrogen sulfide (H_2S) is important because of toxicity, corrosion, and odor nuisance concerns. H_2S is generated in large amounts in coal and natural gas processing, petroleum industries, biogas production, and sewage treatment plants.[1] The odor threshold of H_2S is around 3 ppb in air which is well below any known toxic effects, while the threshold limit value (TLV) was set to 10 ppm; at concentrations exceeding 150 ppm, H_2S is extremely toxic and hazardous.[2] Hence, it is important to develop sensors that can monitor H_2S in real time and can detect concentrations from as low as a few parts per billion to the several hundred parts per million in air. A number of H_2S detection techniques have been developed in the past few decades, with electrochemical detection as the most widely utilized method in compact and portable H_2S gas monitors.[3,4] These devices often rely on solid state sensors made of semiconducting metal oxides such as tungsten oxide and tin oxide or metals such as gold. H_2S detection is usually based on determining conductivity changes of thin films upon exposure to H_2S gas.[4,5] While there are a number of successful devices available commercially, drawbacks of existing H_2S monitors include high power consumption (e.g., in metal oxide sensors that require high operating temperatures); low sensitivity, making them unsuitable for environmental monitoring; short lifetime (usually less than one year); short linear dynamic range; interference from other gases (e.g., NH_3, NO_x, etc); and high cost.[6]

Recently, chemical sensors based on one-dimensional nanostructures such as bare or functionalized semiconducting single-walled carbon nanotubes (SWNTs),[6,7] metal oxides, and conducting polymer nanowires[8] have attracted a great deal of attention because of their superior sensing performance. In particular, these sensors offer promising perspectives for real-time monitoring of gases or vapors with high sensitivity and low-power consumption and potentially at a low cost.[6] Their small size will also allow future integration with low-power microelectronics.

* To whom correspondence should be addressed. E-mail: myung@engr.ucr.edu (N.V.M.); marc.deshusses@duke.edu (M.A.D.).

† University of California-Riverside.

‡ Duke University.

(1) (a) Watts, S. F. *Atmos. Environ.* **2000**, *34*, 761–779. (b) Gabriel, D.; Deshusses, M. A. *Proc. Natl. Acad. Sci. U.S.A.* **2003**, *100*, 6308–6312.

(2) (a) Beauchamp, R. O.; Bus, J. S.; Popp, J. A.; Boreiko, C. J.; Andjelkovich, D. A. *CRC Crit. Rev. Toxicol.* **1984**, *13*, 25–97. (b) Glass, D. C. *Ann. Occup. Hyg.* **1990**, *34*, 323–327.

(3) (a) Sedlak, J. M.; Blurton, K. F. *Talanta* **1976**, *23*, 445–448. (b) Bergman, I. *J. Electroanal. Chem.* **1983**, *157*, 59–73. (c) Opekar, F.; Bruckenstein, S. *Anal. Chem.* **1984**, *56*, 1206–1209. (d) Redondo, R.; Cunha Machado, V.; Baeza, M. M.; Lafuente, J.; Gabriel, D. *Anal. Bioanal. Chem.* **2008**, *391*, 789–798.

(4) (a) Tao, W. H.; Tsai, C. H. *Sens. Actuators, B* **2002**, *81*, 237–247. (b) Lin, H. M.; Hsu, C. M.; Tang, H. Y.; Lee, P. Y.; Yang, C. C. *Sens. Actuators, B* **1994**, *22*, 63–68. (c) Kersen, U.; Holappa, L. *Anal. Chim. Acta* **2006**, *562*, 110–114. (d) Sberveglieri, G.; Groppelli, S.; Nelli, P.; Perego, C. *Sens. Actuators, B* **1993**, *15/16*, 86–89.

(5) Yoo, K. S.; Sorensen, I. W.; Glaunsinger, W. S. *J. Vac. Sci. Technol., A* **1994**, *12*, 192–198.

(6) Zhang, T.; Mubeen, S.; Myung, N. V.; Deshusses, M. A. *Nanotechnology* **2008**, *19*, 332001.

(7) (a) Kong, J.; Chapline, M. G.; Dai, H. *Adv. Mater.* **2001**, *13*, 1384–1386. (b) Qi, P.; Vermesh, O.; Grecu, M.; Javey, A.; Wang, Q.; Dai, H. *Nano. Lett.* **2003**, *3*, 347–351. (c) Kong, J.; Franklin, N. R.; Zhou, C.; Chapline, M. G.; Peng, S.; Cho, K.; Dai, H. *Science* **2000**, *287*, 622–625. (d) Zhang, T.; Nix, M. B.; Yoo, B. Y.; Deshusses, M. A.; Myung, N. V. *Electroanalysis* **2006**, *18*, 1153–1158.

(8) (a) Kolmakov, A.; Zhang, Y.; Cheng, G.; Moskovits, M. *Adv. Mater.* **2003**, *15*, 997–1000. (b) Xue, X. Y.; Chen, Y. J.; Liu, Y. G.; Shi, S. L.; Wang, Y. G.; Wang, T. H. *Appl. Phys. Lett.* **2006**, *88*, 201907. (c) Wang, J.; Bunimovich, Y. L.; Sui, G.; Savvas, S.; Wang, J.; Guo, Y.; Heath, J. R.; Tseng, H. R. *Chem. Commun.* **2006**, 3075–3077. (d) Liu, H.; Kameoka, J.; Czaplewski, D. A.; Craighead, H. G. *Nano. Lett.* **2004**, *4*, 671–675. (e) Zhang, D.; Li, C.; Liu, X.; Han, S.; Tang, T.; Zhou, C. *Appl. Phys. Lett.* **2003**, *83*, 1845–1847.

10.1021/ac901871d
Published on Web 12/07/2009

There has been only few gas nanosensors developed for H_2S detection. Sun et al.[9] reported a catalytic chemiluminescence sensor made of α-Fe_2O_3 nanotubes for rapid and selective detection of H_2S down to 10 ppm H_2S. However, it required heating to over 110 °C for catalytic oxidation of H_2S to occur as well as complex electronics for chemiluminescence measurement. Geng et al.[10] demonstrated that suppressed electron hoping occurred in gold nanoparticles after exposure to pure H_2S. Although the sensors do not appear to be suitable for monitoring purposes because of low sensitivity, the study provided some mechanistic insight. Recently, we reported on the synthesis and H_2S gas sensing performance of networks made of hybrid polyaniline (PANI) nanowires and gold nanoparticles.[11] Template-free electrochemical polymerization was used to synthesize 250−320 nm diameter PANI nanowires that were then decorated with gold nanoparticles by electrodeposition. The nanostructures exhibited superior H_2S gas sensing, with a detection limit of 0.1 ppb H_2S in air at room temperature and a linear response from 0.1 to 500 ppb. However, polymer-based sensors are often subject to drift over time and have a low operating temperature range.[8]

In this report, we demonstrate site-specific electrodeposition of gold nanoparticles on SWNT networks and use these nanostructures to study the mechanisms and demonstrate the effectiveness of H_2S gas sensing at room temperature. SWNTs were selected as templates for growing nanoparticles because of their unique physical and chemical properties along with their ultra high surface area to volume ratio. Also SWNTs have little or no chemical interaction with H_2S or other gases that may interfere.[6] By varying the electrodeposition conditions, gold nanoparticles of different diameter and density were deposited. The sensor synthesis conditions were optimized to enhance H_2S sensing performance. Sensing data suggested that the adsorption of H_2S molecules onto the gold nanoparticle surface altered the work function of the gold which in turn altered the carbon nanotube conductivity.

METHODS

Nanosensor Fabrication. Sensor arrays were microfabricated as described previously[12] on a silicon substrate using standard lithographic patterning. Approximately 1 μm thick SiO_2 film was first deposited on a lightly doped p-type (100) oriented silicon wafer using chemical vapor deposition (CVD) to insulate the substrate. The electrode area was defined by photolithography using positive photoresist, followed by e-beam evaporation of a 20 Å-thick Cr adhesion layer and a ~3000 Å-thick gold layer. Finally, electrodes (200 μm × 200 μm), separated by a gap of approximately 5 μm, were defined using lift-off techniques. To fabricate SWNT interconnects across the electrodes, first, carboxylated-SWNTs (SWNT-COOH 80−90% purity) (Carbon Solution, Inc. Riverside, CA) were dispersed (1 μg/mL) in dimethyl formamide (DMF, Sigma Aldrich, MO) using ultrasonic force for 60 min. Then, 50 nL of the SWNT solution was manually dispensed on top of the electrode gap using a microsyringe. After the evaporation of the solution, a network of randomly oriented SWNTs bridged each electrode gap. Atomic force microscopy observation of the networks (not shown) revealed that 80% of the SWNTs or SWNT bundles were in the 3−5 nm diameter range, with lengths ranging from a few micrometers to about 10−20 μm. The sensors were then annealed at 300 °C for 30 min under a reducing atmosphere (5% H_2 + 95% N_2) to minimize the contact resistance between the CNT network and the gold pads and to remove any DMF residues. The number of SWNTs bridging the electrode gap was controlled by adjusting the concentration of the SWNTs in the DMF solution and the droplet size.

Electrochemical Functionalization. Electrodeposition of gold nanoparticles on the SWNT networks was performed using three electrode electrochemical cell configurations. The linear sweep voltammetry (LSV) and chronoamperometry (potentiostatic) measurements were carried out using a VMP2-potentiostat (Princeton Applied Research, Oak Ridge, TN). For particle characterization studies, gold nanoparticles were electrodeposited on spray printed SWNT film on gold substrates. Commercially available ready-to-use gold electroplating solution from Technic Inc. (Techni-gold 25 ES, CA) was used as electrolyte. Spray printed SWNT films on gold electrodes served as the working electrode, and Pt mesh as counter and standard glass Ag/AgCl (saturated KCl) served as the reference electrode. The apparent surface area of electrode was fixed at 1 cm^2. For gas sensing studies, first, a 3 μL droplet of Au electrolyte solution was placed on top the SWNT network bridging the electrode gap. An alkaline cyanide-free gold electrolyte (pH = 7.5) was selected to prevent the dissolution of a Cr adhesion layer which can be readily attacked in an acidic environment. Next, platinum and Ag/AgCl wires were positioned inside the droplets using a micropositioner. The annealed SWNT networks along with the gold electrodes served as the working electrodes, while platinum and Ag/AgCl wires served as the counter and pseudo reference electrodes, respectively. All depositions were carried out in potentiostatic mode (constant potential) at 25 °C and ambient pressure, with deposition charge as the stopping criteria. After deposition, the electrodes were rinsed with deionized water and acetone to remove any metal salt residues and impurities.

Characterization. The size and number of gold nanoparticles on SWNTs were determined using field emission-scanning electron microscopy (Leo model # 1550, Peabody, MA) and atomic force microscopy (PSIA, Inc. model # XE100, Santa Clara, CA). Atomic force microscopy (AFM) images were obtained using a noncontact mode at a very low scan rate (0.1 Hz) for accurate representation of particle size and density. Five sets of functionalized SWNT networks (5 μm by 5 μm) were selected for particle size and density determinations. For measuring the particle size, particle height was measured rather than particle width to avoid AFM tip convolution effects. A good agreement was observed with the particle width measurement obtained from SEM images, indicating that nanoparticles formed on the SWNTs were more or less spherical in shape. The temperature dependent electrical transport properties of Au-SWNTs were characterized using a Physical Property Measurement System from Quantum Design,

(9) Sun, Z.; Yuan, H.; Liu, Z.; Han, B.; Zhang, X. *Adv. Mater.* **2005**, *17*, 2993–2997.

(10) Geng, J.; Thomas, M. D. R.; Shephard, D. S.; Johnson, B. F. G. *Chem. Commun.* **2005**, 1895–1897.

(11) Shirsat, M. D.; Bangar, M. A.; Deshusses, M. A.; Myung, N. V.; Mulchandani, A. *Appl. Phys. Lett.* **2009**, *94*, 083502.

(12) Mubeen, S.; Zhang, T.; Yoo, B. Y.; Deshusses, M. A.; Myung, N. V. *J. Phys. Chem. C* **2007**, *111*, 6321–6327.

Inc. (San Diego, CA), and I−V characteristics were determined using a semiconductor parameter analyzer (HP model # 4155A, Palo Alto, CA).

Gas Sensing Studies. For gas sensing studies, the sensors were wire bonded, and each sensor was connected in series with a load resistor. The value of the load resistor was chosen to be as close as possible to the initial sensor resistance to optimize the resolution obtained from the measurements. The sensors typically had a baseline resistance in the range of 20 KΩ at room temperature. This baseline resistance value was selected on the basis of optimization studies carried out earlier.[12] The circuit was subjected to a fixed voltage, and the electrical resistance of the sensor was determined by continuously monitoring the differential voltage over the load resistor and applying Ohm's law. The applied voltage across the sensor was varied from 1 to 5 V to study the effect of applied bias on sensing performance.

A 3.6 cm^3 sealed glass chamber with gas inlet and outlet ports for gas flow through was positioned over the sensor chip. All experiments were conducted with hydrogen sulfide (purity: 99.998%) diluted in dry air (purity: 99.998%) at a gas flow of 200 std. cm^3 min^{-1}. The H_2S and dry air gas flow rates were regulated by mass flow controllers (Alicat Scientific Incorporated, Tucson, AZ). A custom Lab view computer program was developed to continuously control and monitor the voltage of the circuit using field point analog input and output modules (National Instruments, Austin, TX). In all the experiments, sensors were first exposed to air to obtain the baseline, then to a desired concentration of H_2S gas, and then back to air, which completed one cycle.

RESULTS AND DISCUSSION

Effect of Deposition Parameters on Metal Deposition. For topographic studies, gold nanoparticle electrodeposition was conducted at constant potential mode. The deposition potential and duration were varied, and gold nanoparticle size and density were determined. Figure 1A shows a typical LSV obtained for gold deposition on spray printed SWNTs. For all these determinations, high density SWNT networks on gold substrate were used instead of actual sensors, for easier optimization purposes. Also, for spray printed SWNTs, the electrolyte is mainly in contact with the surface of SWNTs; therefore, any changes observed during electrodeposition studies is attributed to changes occurring on the surface of SWNTs instead of the gold electrodes. The LSV indicated that electrodeposition of gold on SWNTs started when the applied deposition potential became more negative than −0.4 V (vs Ag/AgCl) where the cathodic current sharply increased. The effect of deposition potential on particle size and density for a constant charge passed (1 mC/cm^2) is shown in Figure 1B. Low overpotentials (−0.4 to −0.5 V vs Ag/AgCl) resulted in low deposition rate and led to small and sparsely dispersed gold nanoparticles, suggesting that nucleation was mostly taking place at the SWNT defect sites.[13] This is consistent with the observation of an energetic barrier for nucleation on defect free SWNT surfaces.[14] At more negative overpotentials, both the size of the deposits and coverage by gold nanoparticles increased due to an increased deposition rate. As the size of the deposits increased,

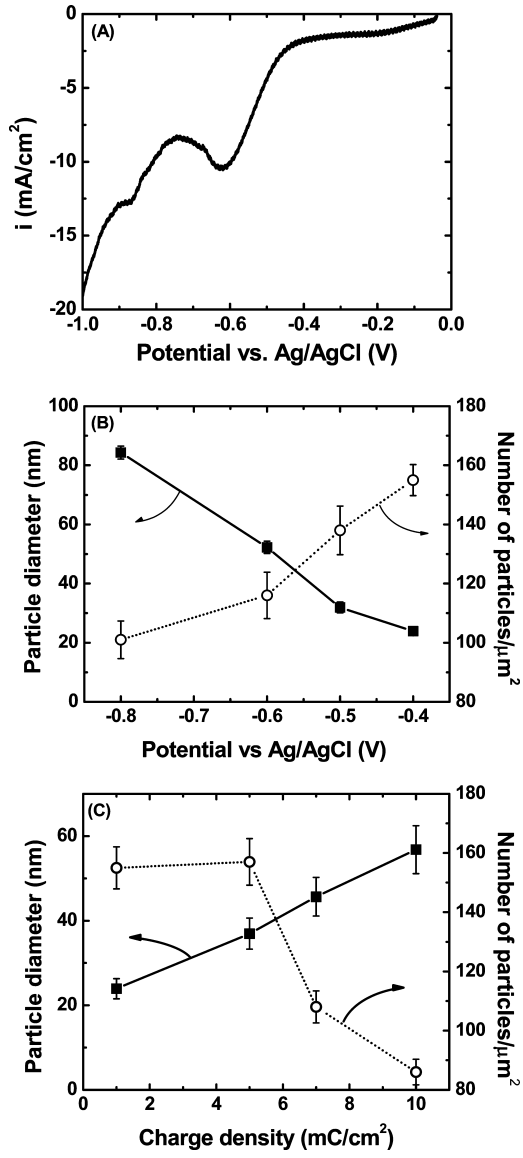

Figure 1. Effect of electrodeposition parameters on nanoparticle size and density: (A) linear sweep voltammogram of gold nanoparticle deposition on spray-printed SWNTs (1 cm^2). The scan rate was fixed at 10 mV/s. The reference was a standard Ag/AgCl electrode (saturated KCl). Effect of deposition potential (B) and charge density (C) on gold nanoparticles size and density on spray printed SWNTs. The charge density was fixed at 1 mC/cm^2 for (B) and deposition potential was fixed at −0.4 V for (C).

significant metal particle coalescence was observed. This implied that metal clusters were being deposited on SWNTs rather than deposition as a monolayer, which is not typical of deposition onto surfaces having lower interfacial energies.[15]

The effect of deposition time on particle size and density was determined at a fixed potential (Figure 1C). For this experiment, a low cathodic deposition potential was selected (−0.4 V vs Ag/AgCl), as it resulted in the smallest deposits. The particle density remained constant at lowest charge densities (1−5 mC/cm^2) consistent with the hypothesis that gold initially deposits at the SWNT defect sites. A sharp decrease in particle density

(13) Fan, Y.; Goldsmith, B. R.; Collins, P. J. *Nat. Mater.* **2005**, *4*, 906–911.
(14) Walter, E. C.; Favier, F.; Penner, R. M. *Anal. Chem.* **2002**, *74*, 1546–1553.
(15) (a) Penner, R. M. *J. Phys. Chem. B* **2002**, *106*, 3339–3353. (b) Zoval, J. V.; Stiger, R. M.; Biernacki, P. R.; Penner, R. M. *J. Phys. Chem.* **1996**, *100*, 837–844.

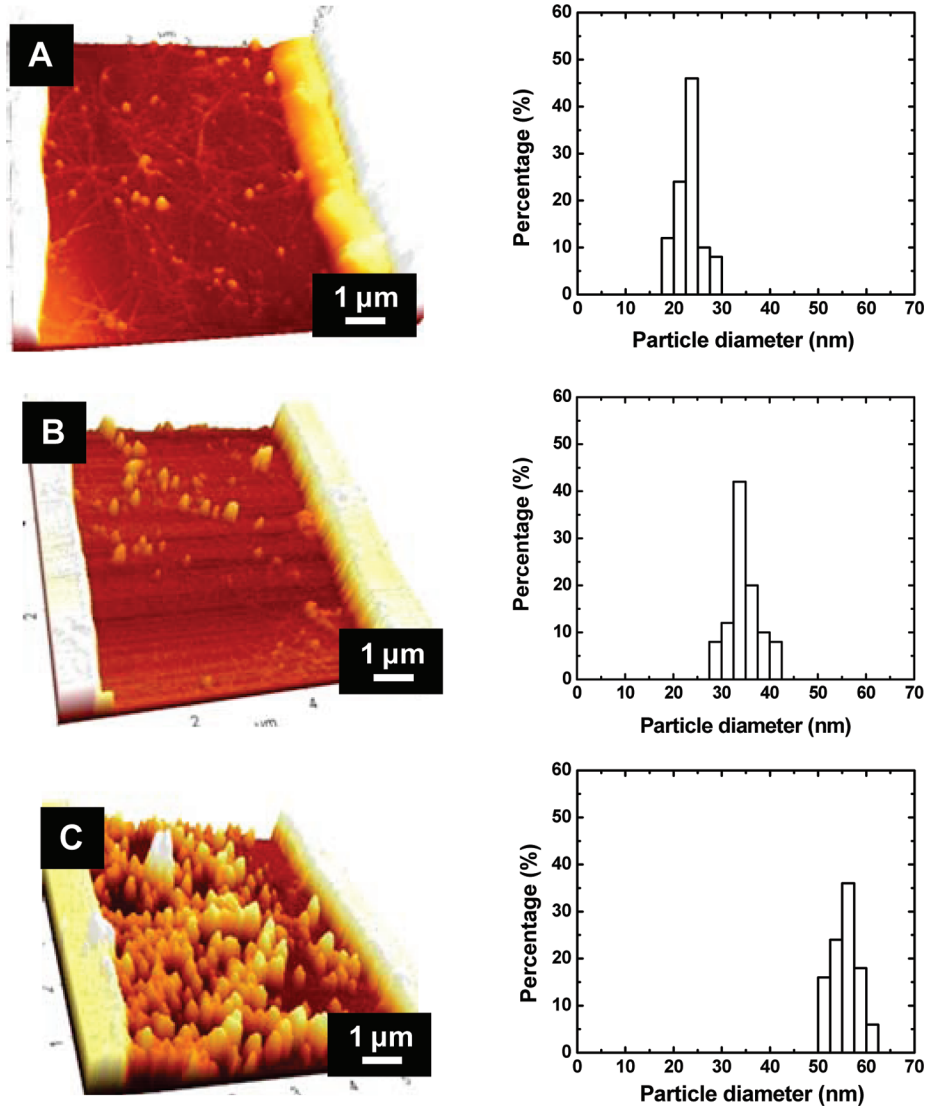

Figure 2. AFM images and histograms of gold nanoparticle decorated SWNTs with different charge density: (A) 1 mC/cm^2, (B) 5 mC/cm^2, and (C) 10 mC/cm^2. The deposition potential was fixed at −0.4 V versus the pseudo reference electrode (chlorinated Ag/AgCl wire). The initial resistance of SWNTs before decoration was in the range of 10−40 KΩ.

was observed as the charge density was increased, most probably because there was coalescence of the deposits as they grew in size. The particle diameter increased with charge density similar to earlier experiments in which palladium was deposited on SWNTs,[12] except that, here, a quasi-linear increase was observed. The observations are consistent with AFM images and gold deposit size histograms sensors shown in Figure 2. AFM images at low charge densities (Figures 2AB) show that gold deposits are clearly located on the SWNTs. As the charge density increased, larger gold clusters and greater coverage of the SWNTs with gold deposits were observed. At 10 mC/cm^2, extensive coverage of the sensing area with gold deposits is accomplished. Examination of the deposit size histograms reveals that the size distribution remained relatively constant with the charge density. This is probably because the number of nucleation sites is not affected by the charge density.

Overall, the results of Figures 1 and 2 show that electrodeposition allows one to precisely control the size and density of the metal nanoparticle deposits by varying the charge density and the deposition potential.

The room temperature I−V characteristics of randomly oriented carboxylated SWNTs and gold nanoparticle decorated SWNTs are shown in Figure 3A. For carboxylated SWNTs and those with a low density of gold deposits, the I−V characteristics are S-shaped, indicating Schottky contacts which are usually observed for SWNTs on gold pads. However, as was shown in Figure 2C, at the higher density of gold deposits, the nanotubes are almost continuously covered with nanoparticles forming a gold nanowire or a filmlike structure, and consequently, a linear Ohmic behavior is observed for dense deposits. The temperature dependent resistance characteristics provided further insight on the conduction path of electrons across the source and drain electrodes. For sparse gold nanoparticle deposits, the resistance of the device increased with a decrease in temperature, indicating that the current conduction path is through the semiconducting SWNTs (Figure 3B), while at a high deposit density; the resistance decreased with a decrease in temperature which is a characteristic feature of metals. This indicated that the underlying SWNTs no longer played a role in the conduction path and that conduction

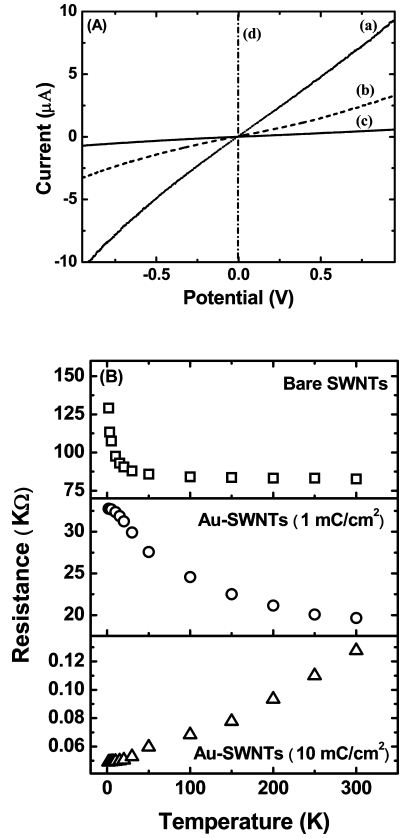

Figure 3. I−V characteristics (A) and temperature dependent electrical resistance (B) of Au-SWNTs as a function of deposition charge density. (a) Carboxylated SWNTs, Au-SWNTs with a charge density of (b) 1 mC/cm^2, (c) 5 mC/cm^2, and (d) 10 mC/cm^2. All the devices were made at a constant deposition potential of −0.4 V versus chlorinated Ag/AgCl wire.

was through a continuous gold wire. The thermal activation energy of the devices for the low density deposit case, calculated by plotting ln R vs $1/T$ (see Figure S1 in the Supporting Information), was found to be about 3.5 meV, which is comparable to the thermal activation energy value of 5 meV for Pd decorated SWNTs[12] and 6 meV for carboxylated SWNT networks.[16] The activation energy values further confirm that the dominant conduction pathway in sparsely decorated networks is across the semiconducting nanotubes and/or due to the tunneling barriers between the nanotube networks.

H_2S Gas Sensing. For H_2S sensing studies, three topographically different sensors were selected: (i) sensors with the smallest gold particle diameter (−0.4 V, 1 mC/cm^2), (ii) sensors with the same particle density but about a 2-fold larger gold particle (−0.4 V, 5 mC/cm^2), and (iii) sensors with large and dense gold deposits and overall metallic behavior (−0.4 V, 7 mC/cm^2). Figure 4A shows the dynamic responses of these sensors compared to the response of carboxylated SWNTs for two repeated exposures to 20 ppb H_2S at room temperature. The carboxylated SWNTs have no chemical interaction with H_2S; hence, no change in the resistance of the device was observed (Figure 4A (a)). This also indicates that the gold pads did not exhibit any response to H_2S exposure at such low concentrations. The resistance of SWNT decorated with gold nanoparticles sharply increased upon exposure to H_2S; the effect was most pronounced for the sample with the smallest size and largest number of nanoparticles (Figure 4A (d)). The increase in resistance observed here is consistent with the measured increase in resistance in gold films[5] and nanoparticles[10] attributed to reduced electron hopping, while a recent nanosensor made with polyaniline (PANI) nanowires decorated with gold nanoparticles exhibited a decrease in resistance when exposed to H_2S.[11]

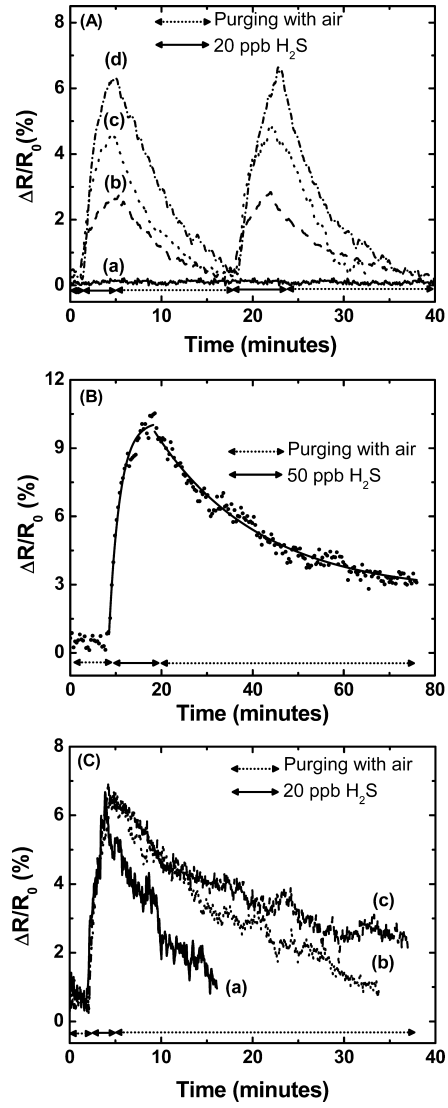

Figure 4. Sensor response (A) to 20 ppb H_2S at room temperature for (a) carboxylated SWNTs and gold decorated SWNT with the following charge deposited: (b) 7 mC/cm^2, (c) 5 mC/cm^2, and (d) 1 mC/cm^2. (B) Resistance change of Au-SWNT sensors to 50 ppb H_2S. Dotted lines are experimental data while the solid line is a fit using the kinetic model developed by Lee et al.[21] (C) Sensor response (−0.4 V, 1 mC/cm^2) to 200 ppb H_2S for different applied bias potentials: (a) 4 V, (b) 2.5 V, and (c) 1.0 V.

The sensing mechanism here is due to change in the electronic structure at the gold-SWNT interface, resulting from the modification of the electronic properties of the gold nanoparticles upon exposure to H_2S gas. H_2S is known to adsorb strongly onto gold because of the high chemical affinity between gold and sulfur.[10] Leavitt and Beebe found that H_2S adsorb (85 K) and desorb molecularly (165 K) at low temperatures from Au (111)

(16) Zhou, C.; Kong, J.; Dai, H. *Phys. Rev. Lett.* **2000**, *84*, 5604–5607.

surfaces.[18] At such low temperatures, H_2S binds weakly to the gold surface; hence, it easily undergoes adsorption and desorption processes molecularly. However, at higher temperatures ($165 < T < 520$ K), Leavitt and Beebe found that adsorbed H_2S decomposes to form SH which is chemisorbed onto the gold surface while H_2 is released. The adsorbed SH remained adsorbed on the gold surface until the onset of even greater temperatures (>520 K) at which SH undergoes disproportionation to form H_2S and adsorbed sulfur still bound to the gold surface. The latter can be removed as elemental sulfur at temperatures above 900 K. With respect to electronic properties, it has been reported that gold−sulfur bonds in alkylthiol self-assembled monolayers can lower the surface work function of gold by as much as 1 eV.[19] Thus, we propose the following sensing mechanism. During electrodeposition, gold nanoparticles are preferentially deposited on the defect sites of the SWNTs[15] because of the higher surface energy of defect sites compared to clean sp^2 bonded lattice, allowing easier electronic interaction between gold and carbon nanotubes. Upon exposure to H_2S, hydrogen sulfide is chemisorbed on the gold nanoparticles and undergoes decomposition to form either Au−SH or Au−S species on the surface of the particles. This lowers the surface work function of the gold particles. Such changes in the electronic state of the gold nanoparticles cause a change in the extent of electron exchange between the gold and the defect sites of carbon nanotubes. As the work function of the gold is reduced, electrons are donated from the gold to the SWNT. Since the latter is a p-type[20] semiconductor at ambient conditions, this results in an increase in its electrical resistance. We hypothesize that the absence of change in resistance for SWNTs (Figure 4A (a)) is because of the fact that the carboxylated SWNTs bind to the gold pads by Vander Waals forces and no charge transfer or Schottky barrier modulation takes place between the gold pads and the SWNTs when exposed to low concentrations of H_2S, unlike what is happening when gold is deposited on the defect sites of SWNTs. A detailed study on understanding the role of gold nanoparticles and gold contacts in H_2S sensing is currently under investigation; transfer characteristics of Au-SWNT devices operated in field effect transistor (FET) mode are consistent with the proposed mechanism. In addition, no change in resistance was observed when gold nanoparticles formed a continuous wire on the SWNTs (Figure S2 in the Supporting Information). This was because the main conduction path was through the gold nanoparticle wire and any modulation of the SWNT resistance by adsorbed H_2S became irrelevant. The decreasing sensor response with increasing deposition charge density (Figure 4A (b−d)) is attributed to the greater specific interfacial area per unit gold volume of the sensors with the smaller gold nanoparticles and to the larger effect of short-range electronic interactions discussed above.

We also investigated the molecular sensing mechanism for H_2S on gold decorated SWNTs using previously reported semitheoretical models.[7b,21] Rate constants for H_2S adsorption can be extracted from a highly simplified model developed by Lee and Strano[21] based on reversible adsorption kinetics of the analyte. The model equations for adsorption and desorption kinetics were fitted to the experimental data (Figure 4B) to extract the rate constants. From the fit, the adsorption (k_{ads}) and desorption (k_{des}) rate constants were estimated to be 4.37×10^3 s^{-1} and 0.72×10^{-3} s^{-1}, respectively. The above kinetic constants reflect that H_2S desorption from the gold surface is much slower than its adsorption, consistent with the fact that disproportionation of SH from the gold surface is only favored at high temperatures. The calculated adsorption and desorption rate constants can be indirectly probed to determine the binding energy. The equilibrium rate constant K (k_{ads}/k_{des}) determined is exponentially related to the enthalpy and free energy of the reaction by van-Hoff's relation[22] given in eq 1.

$$\Delta G = -RT\ln K = \Delta H - T\Delta S \quad (1)$$

The entropy change can be assumed constant for the binding event,[22] and hence, at constant temperature, the equilibrium constant is exponentially related to enthalpy. Because the barrier to desorption is much higher compared to the adsorption event, the amount of energy required to desorb a molecule from a surface can be correlated to the enthalpy of binding.[7b] Hence, eq 1 can be rewritten as

$$k_{des} = \exp(-E_B/RT) \quad (2)$$

Where E_B is the binding energy of the molecule and was determined to be 0.19 eV. The binding energy determined experimentally (0.19 eV) is close to the computed values (0.3 eV−0.4 eV) for binding energy of H_2S on gold surfaces.[18]

Significant research efforts have been directed at means to improve the regeneration rate of gas nanosensors, the most common being increasing the operating temperature or UV irradiation.[7b] Here, we tried a different approach. The applied bias potential was increased during sensing in an attempt to improve the regeneration rate. The dynamic responses of a sensor subjected to different applied bias potentials while sensing H_2S are plotted in Figure 4C. The sensor responses to H_2S were almost identical for the three different bias potentials applied. However, recovery to the baseline when switching off H_2S was accelerated with increasing bias potential. Desorption rates improved (0.72×10^{-3} s^{-1} (1 V), 0.3×10^{-1} s^{-1} (2.5 V), 0.6×10^{1} s^{-1} (4 V)) with increasing applied bias. The most probable explanation for the faster recovery at higher bias potentials is the greater local Joule heating at the defect sites with increasing applied bias potential. SWNTs are excellent thermal conducting

(17) Leavitt, A. J., Jr. *Surf. Sci.* **1994**, *314*, 23–33.

(18) (a) Cui, X.; Freitag, M.; Martel, R.; Brus, L.; Avouris, P. *Nano Lett.* **2003**, *6*, 783–787. (b) Schoenenberger, C.; Jorritsma, J. C.; Sondag-Huethorst, J. A. M.; Fokkink, L. G. J. *J. Phys. Chem.* **1995**, *99*, 3259. (c) Alloway, D. M.; Hofmann, M.; Smith, D. L.; Gruhn, N. E.; Graham, A. L.; Colorado, R., Jr.; Wysocki, V. H.; Lee, T. R.; Lee, P. A.; Armstrong, N. R. *J. Phys. Chem. B* **2003**, *107*, 11690. (d) Ah Qune, L. F. N.; Akiyama, H.; Nagahiro, T.; Tamada, K.; Wee, A. T. S. *App. Phys. Lett.* **2008**, *93*, 083109. (e) Sushko, M. L.; Shluger, A. L. *Adv. Mater.* **2009**, *21*, 1111.

(19) (a) Kong, J.; Franklin, N.; Zhou, C.; Chapline, M.; Peng, S.; Cho, K.; Dai, H. *Science* **2000**, *287*, 622–625. (b) Collins, P.; Bradley, K.; Ishigami, M.; Zettl, A. *Science* **2000**, *287*, 1801–1804.

(20) Lee, C. Y.; Strano, S. M. *Langmuir* **2005**, *21*, 5192–5196.

(21) Espenson, J. H. *Chemical Kinetics and Reaction Mechanisms*; McGraw-Hill, Inc.: New York, 1981.

(22) Bohrer, F. I.; Colesniuc, C. N.; Park, J.; Ruidiaz, M. E.; Schuller, I. K.; Kummel, A. C.; Trogler, W. C. *J. Am. Chem. Soc.* **2009**, *131*, 478–485.

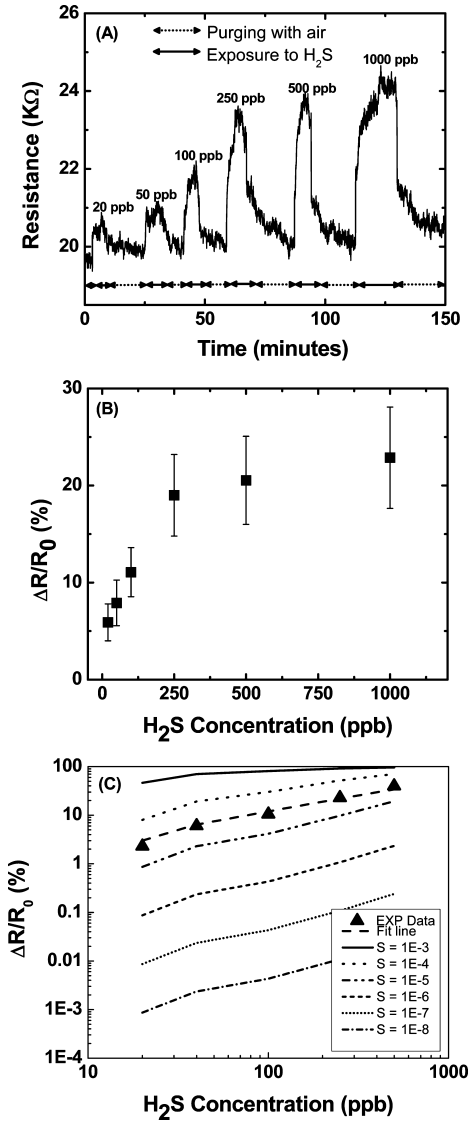

Figure 5. (A) Response of a 20 KΩ Au-SWNT sensor (V_{dep}: −0.4 V, C_{dep}: 1 mC/cm^2) to different H_2S concentrations for an applied bias of 4 V. (B) Resistance change ($\Delta R/R_0$) for different H_2S concentrations and (C) calculated ($\Delta R/R_0$) for Au-SWNT sensor plotted versus H_2S concentration for different sticking coefficients (S). The solid triangles are the experimental data.

materials, but surface defects are known to result in localized phonon scattering and increased Joule heating. Thus, temperature at defect sites should increase with increasing bias potential and the associated Joule heating.

Finally, selected sensors were subjected to different concentrations of H_2S ranging from 20 to 1000 ppb (Figure 5A). In each case, the sensor promptly reached a steady state after exposure to the analyte and returned to its baseline when the analyte gas feed was discontinued. The sensor exhibited a steep and linear ($r = 0.986$) response for concentrations ranging from 20 to 250 ppb (Figure 5B) while saturation was observed above 250 ppb. The sensitivity (defined as sensor response/analyte concentration) was found to be 0.07% per ppb in the linear range. The lower detection limit (defined as the concentration providing a signal-to-noise ratio of at least 3) was 3 ppb which is about the same as odor threshold level for humans. This is higher than our previous report on gold functionalized polyaniline nanowires;[11] however, polymer-based sensors have a low upper temperature range (usually about 60−80 °C) and tend to have a poor stability over time.[8] Further, electrodeposition on conducting polymer can only be made in a narrow range of cathodic potentials, as the polymer can be reduced at excessive potentials, which would affect its conductivity. These limitations do not exist in metal functionalized SWNT-based sensors. The response time was typically in the range of 6−8 min for all selected concentrations, while the recovery time was around 10 min for lower concentrations (20−100 ppb) and almost twice that value for higher H_2S concentrations (200−1000 ppb). This is in the upper middle range of response time for nanomaterial-based gas sensors.[6] The sensors exhibited some cross sensitivity to NH_3. Examination of the responses (see Figure S3 in the Supporting Information) obtained by bare carboxylated SWNTs and Au-SWNTs, when exposed to NH_3 in air, revealed only minor differences. This indicates the Au nanodeposits played no role in the NH_3 sensing response. In contrast, major modulation of sensor resistance was obtained for H_2S exposures. This property could be exploited in sensor arrays in order to discriminate H_2S from interfering gases. The sensors were stable over time, with less than 25% loss in H_2S sensitivity after being stored for 6 months and no major change of the response or recovery times (see Figure S4 in the Supporting Information).

From the above sensing results, the experimental sticking coefficient (ratio of adsorbate molecules that adsorb to the surface to the total number of molecules that reaches the surface for a fixed period of time at fixed temperature) for H_2S was also determined using a Langmuir isotherm model as suggested by Qi et al.[7b] Assuming that the relative change in resistance ($\Delta R/R_0$) is proportional to the adsorption of H_2S molecules on gold nanoparticles, $\Delta R/R_0$ was plotted as a function of H_2S gas concentrations for different sticking coefficients (Figure 5C) from 10^{-3} to 10^{-8}. Examination of the figures reveals that a sticking coefficient for H_2S on a Au-SWNT network of 3×10^{-5} provides an adequate representation of the experimental data. There was less than a 4% change observed for the conductivity of carboxylated SWNTs when exposed to H_2S concentrations as high as 20 ppm (see Figure S3 in the Supporting Information). This indicates that H_2S molecules do not "stick" or adsorb to significant extents on carboxylated SWNTs and that gold functionalization significantly increases the binding affinity of H_2S toward these hybrid nanostructures.

CONCLUSIONS

Novel gas nanosensors consisting of gold nanoparticles electrodeposited on SWNTs were synthesized. The chemiresitive sensors allowed rapid and quantitative detection of trace H_2S concentrations at room temperature. The sensing mechanism is believed to be based on the modulation of the conduction path across the nanotubes, by changing the extent of electron exchange between the gold and the defect sites of nanotubes when exposed to various concentrations of H_2S. Electrochemical functionalization of gold nanoparticles on SWNTs has many advantages including simple processing and site-specific functionalization of nanostructured materials. The sensor characteristics could be tuned by changing the sensor synthesis conditions such as deposition potential, deposition charge, and

initial resistance of the sensor. The SWNTs were functionalized with gold ranging from about 20 nm nanoparticles up to continuous deposits forming a nanowire depending on the deposited charge. The sensors exhibited superior sensitivity toward H_2S (0.07% per ppb at room temperature with a detection limit of 3 ppb) over many conventional gas sensors. Increasing the bias voltage during sensing reduced the sensor recovery time, probably by local Joule heating. Sensors such as the ones presented herein offer tremendous potential for the development of powerful sensor arrays and their integration in low cost monitoring devices.

ACKNOWLEDGMENT

Funding for the project was provided by Bourns, Inc., University of California Discovery Grant (UC Discovery), the Defense Microelectronic Activity (DMEA) under agreement Number H94003-05-2-0505, and the NIH Genes, Environment, and Health Initiative through Award U01 ES 016026.

SUPPORTING INFORMATION AVAILABLE

Plot of ln R vs $1/T$ for low density Au deposit case; response of a high density deposit case sensor to H_2S. Sensing of NH_3 and H_2S by carboxylated and Au-SWNT sensors. Comparison of as-prepared sensor response (25 ppb H_2S in air) and sensor response after 6 months of storage. This material is available free of charge via the Internet at http://pubs.acs.org.

Received for review August 18, 2009. Accepted November 6, 2009.

AC901871D

Supporting Information

Sensitive Detection of H_2S Using Gold Decorated SWNT Nanosensors

Syed Mubeen[1], Ting Zhang[1], Ashok Mulchandani[1], Nosang V. Myung[1] and Marc A. Deshusses[2]**

[1]Department of Chemical and Environmental Engineering and Center for Nanoscale Science and Engineering; University of California-Riverside; Riverside, CA 92521

[2]Department of Civil and Environmental Engineering; Duke University; Durham, NC 27708

Contents:

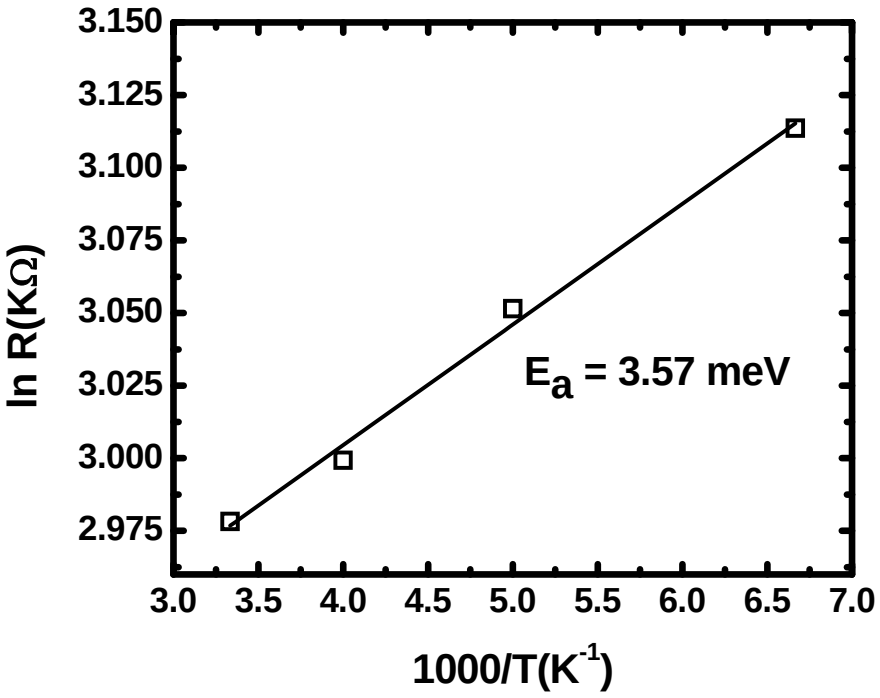

Figure S1. Ln R vs. 1/T curve over a range of 200-300 K for Au-SWNT sample with deposition conditions of 1 mC/cm^2 and -0.4 V versus chlorinated Ag/AgCl wire. The plot shows typical characteristics of semiconductors with an activation energy of 3.57 meV. Activation energy is determined from the formula $\sigma = \sigma_0 \exp(-E_a/K_BT)$.

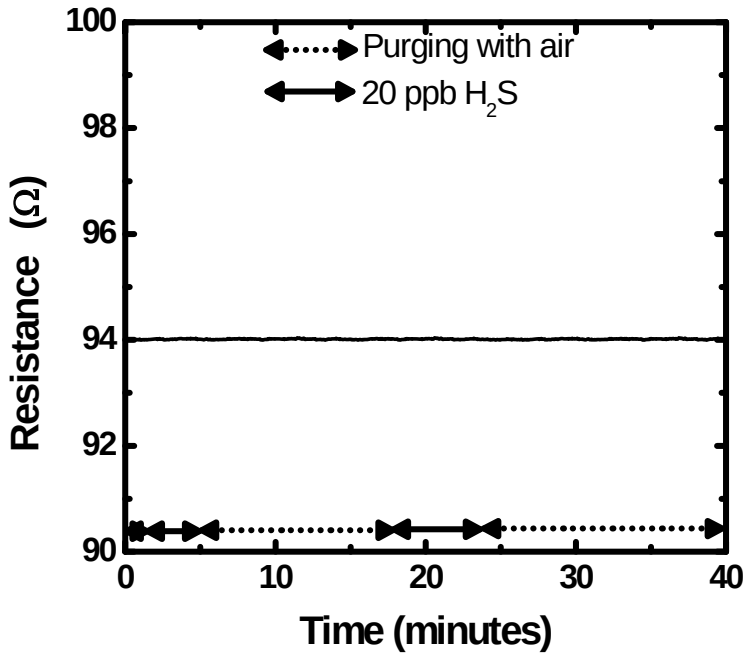

Figure S2. Real time response of a Au-SWNT sensor with 10 mC/cm^2 Au deposited at -0.4 V vs. chlorinated Ag/AgCl wire to repeated exposures (arrows) of 20 ppb H_2S at room temperature. No change in resistance was observed.

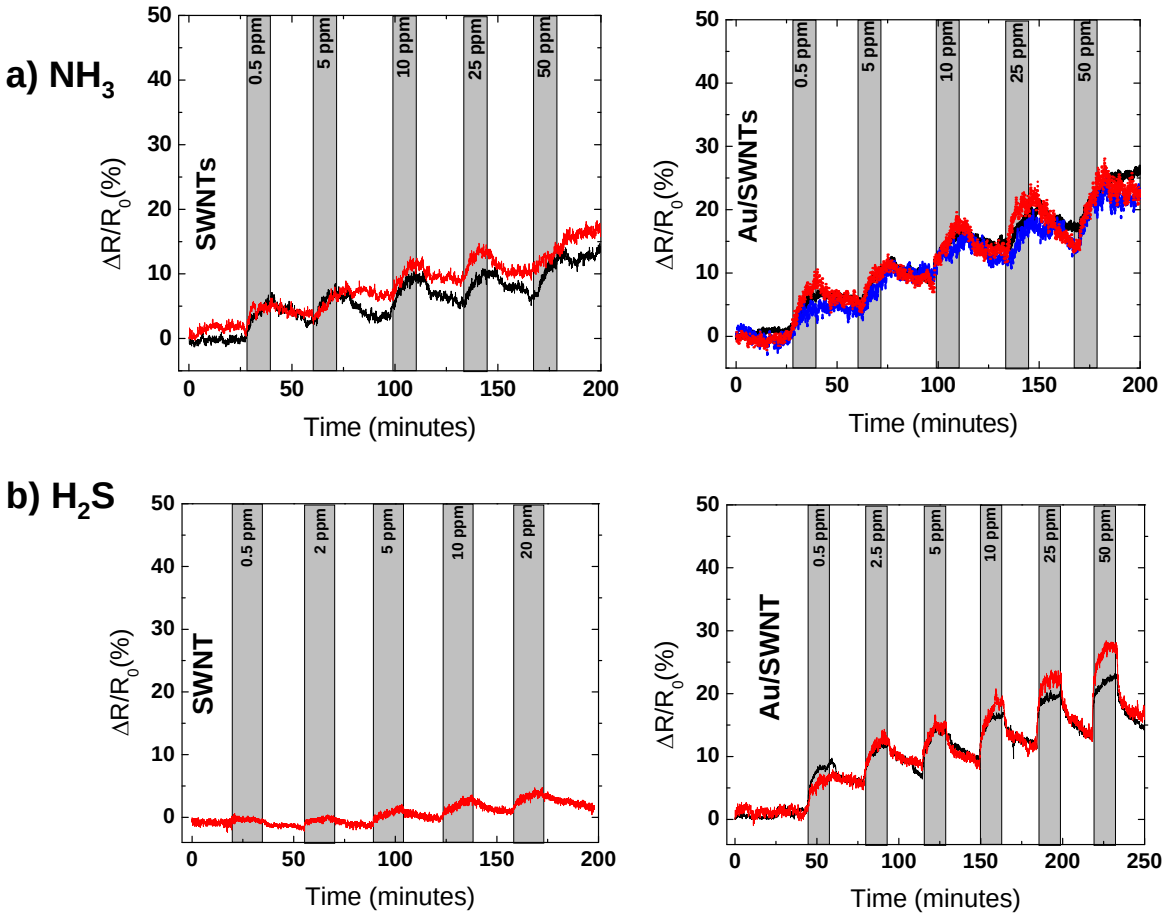

Figure S3. Comparison of sensing responses of duplicate bare carboxylated SWNT sensors (left) and Au-SWNT sensors (right) to increasing concentrations of NH_3 and H_2S.

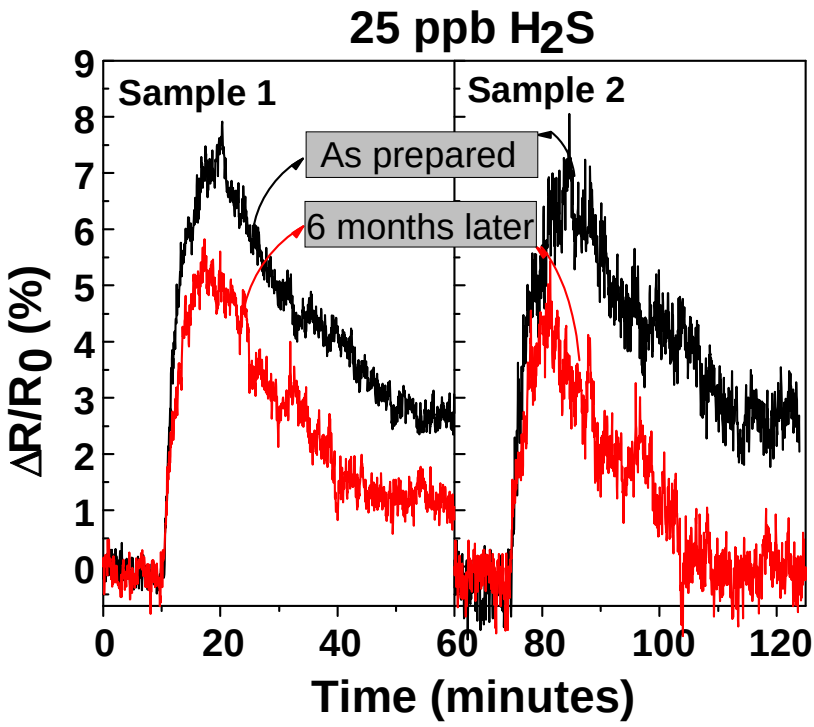

Figure S4. Comparison of sensing performance for 25 ppb H_2S in dry air for as-fabricated Au-SWNTs sensor and the same sensor after six months.